# Dynamics of the Establishment of Systemic Potyvirus Infection: Independent yet Cumulative Action of Primary Infection Sites

**Guillaume Lafforgue, Nicolas Tromas, Santiago F. Elena and Mark P. Zwart**

***J. Virol.*** **2012, 86(23):12912. DOI: 10.1128/JVI.02207-12.**
**Published Ahead of Print 19 September 2012.**

JVI Journals.ASM.org

# Dynamics of the Establishment of Systemic *Potyvirus* Infection: Independent yet Cumulative Action of Primary Infection Sites

**Guillaume Lafforgue,[a] Nicolas Tromas,[a] Santiago F. Elena,[a,b] and Mark P. Zwart[a]**

Instituto de Biología Molecular y Celular de Plantas, Consejo Superior de Investigaciones Científicas-UPV, València, Spain,[a] and The Santa Fe Institute, Santa Fe, New Mexico, USA[b]

**In the clinic, farm, or field, for many viruses there is a high prevalence of mixed-genotype infections, indicating that multiple virions have initiated infection and that there can be multiple sites of primary infection within the same host. The dynamic process by which multiple primary infection sites interact with each other and the host is poorly understood, undoubtedly due to its high complexity. In this study, we attempted to unravel the basic interactions underlying this process using a plant RNA virus, as removing the inoculated leaf can instantly and rigorously eliminate all primary infection sites. Effective population size in the inoculated leaf and time of removal of the inoculated leaf were varied in experiments, and it was found that both factors positively influenced if the plant became systemically infected and what proportion of cells in the systemic tissue were infected, as measured by flow cytometry. Fitting of probabilistic models of infection to our data demonstrated that a null model in which the action of each focus is independent of the presence of other foci was better supported than a dependent-action model. The cumulative effect of independently acting foci therefore determined when plants became infected and how many individual cells were infected. There was no evidence for interference between primary infection sites, which is surprising given the planar structure of leaves. By showing that a simple null model is supported, we experimentally confirmed—to our knowledge for the first time—the minimal components that dictate interactions of a conspecific virus population establishing systemic infection.**

Viral infection of a complex multicellular host usually begins with the infection of a small number of cells (32, 36). From this site of primary infection, the virus then expands into other tissues, often making use of the host's vasculature. In some cases, this expansion eventually becomes irremediable on a small spatiotemporal scale; local host defenses are no longer able to contain infection, and the virus is established at the main sites of replication, a state that is generally referred to as systemic infection. In many viral pathosystems, the transition from primary infection to systemic infection is labyrinthine: the host immune system effectuates different defensive mechanisms, and on the other hand, different infection pathways are accessible to the virus (10, 23). This great complexity has made it difficult to study interactions within the virus population during the establishment of systemic infection. Different expanding viral populations within the host could conceivably have antagonistic or synergistic effects on one another, in conjunction with the host immune system. In other words, if there are multiple sites of primary infection in a single host, how will these nascent infections affect each other?

Experimental evidence suggests that the independent-action (IA) model may be generally applicable to the viral infection process (33, 35, 36, 38). The IA model assumes that each virion has a nonzero probability of infecting the host and that this probability of infection is not affected by the number of virions present in the inoculum (2, 9, 38). Corollaries of IA have been experimentally demonstrated: one or a small number of virions can cause systemic infection (1, 3, 28, 33, 36, 38), and viral effective population size ($N_e$) is dose dependent (36). Tests of IA have, however, focused on qualitative outcomes of infection (i.e., whether a particular host is infected and which viral genotypes are present at the end of infection) and not on infection dynamics. In this study, we therefore addressed the question of whether the principle of independence still holds when temporal processes are considered. Note that from the outset, we limited the scope of our study to the concurrent infection of a host organism with a conspecific viral population; we did not consider interactions between distinct genotypes or noninstantaneous exposure to a virus (i.e., superinfection). An alternative to IA is a dependent-action (DA) model, in which primary infection sites interact with one another during the dynamic process of establishing systemic infection. Two sorts of DA interactions are possible. If primary infection sites have a negative effect on each other, there is antagonistic dependent action (ADA), whereas if primary infection sites have a positive effect on each other, there is synergistic dependent action (SDA).

One particularly interesting dynamic process during viral infection is the transition from primary to systemic infection. For plant viruses, viral infection begins with the infection of a relatively small number of cells in the inoculated or exposed leaf (1, 3, 25, 29, 36). However, many hurdles must be surpassed before systemic infection of the plant is established. Indeed, several steps are required, starting with expansion from a single infected epidermal cell to adjacent tissue such as mesophyll, bundle sheath, or phloem parenchyma/companion (5) by means of relatively slow cell-to-cell movement (6, 15). Infection of companion cells to sieve elements (8) offers access to long-distance transport within the plant, allowing for rapid expansion to distant tissues (24). Only by establishing systemic infection can a plant virus be readily accessible to vectors and ensure its transmission to new hosts. Virions loaded into phloem are responsible for long-distance

**Received** 17 August 2012 **Accepted** 11 September 2012
**Published ahead of print** 19 September 2012
Address correspondence to Mark P. Zwart, marzwa@upvnet.upv.es.
G.L. and N.T. contributed equally to this article and are listed in alphabetical order.

doi:10.1128/JVI.02207-12

movement in our model system, *Tobacco etch virus* (TEV; genus *Potyvirus*, family *Potyviridae*). We therefore use the term virion to describe the unit of long-distance movement, although the equivalent in some other plant viruses would be the movement nucleoprotein complex. In the case of TEV, the transition from primary infection to systemic infection has a probability very near 1 (36). Even in this case, however, if the dynamic process is considered, then independence in the establishment of systemic infection may be rejected. One factor likely to contribute to the undoing of independence is spatial constraints in viral expansion, as the potyviruses show little cellular coinfection, reportedly leading to spatial separation (7). The host plant leaf is a largely two-dimensional surface, and hence viruses of equal fitness can exclude each other from systemic infection, one virus blocking another's access to host vascular tissue even when the viruses are coinoculated (36).

Plant viruses are well suited as experimental model systems to study the population biology of the infection process (2, 12–14, 16–18, 26, 27). Moreover, plant viruses have unique advantages for studying the transition from primary to systemic infection. First, plant viruses have historically been exploited for their ability to induce local lesions (2) and, more recently, primary infection foci (36) which could be quantified and used to model infection. It is therefore possible to estimate $N_e$ without disrupting infection, meaning that $N_e$ can be related to downstream processes in the same plant (e.g., systemic infection). Second, when plants are mechanically inoculated, the sites of primary infection are restricted to the inoculated surface. As the removal of a leaf has limited effects on the host plant, it is therefore possible to stringently and instantaneously remove all primary infection sites at a specific time postinoculation. This property of plant-virus pathosystems has also been historically exploited, as this basic experimental setup had already been reported in 1924 (31). Whether systemic infection occurs will, then, depend on virions that have already been loaded in the phloem and have egressed the inoculated leaf prior to its removal. We therefore used a plant virus, TEV, to study how $N_e$ and the time of removal of the inoculated leaf affect the probability of the occurrence of systemic infection and to determine what interactions exist between primary infection foci and with the host plant. We also wanted to quantitatively relate $N_e$ and the time of removal to downstream events in the systemically infected tissue. Plant virus infection is generally quantified by molecular biology techniques such as real-time quantitative reverse transcription-PCR (RT-qPCR) (4) or biological measures such as lesion-forming units (2, 22). Neither technique indicates the proportion of infected cells, while RT-qPCR measures not viable particles but, rather, viral RNA produced. We therefore developed an innovative new approach to determine directly the infectious status in thousands of individual cells based on translation of a protein encoded by the virus: flow cytometry on protoplasts isolated from systemically infected tissue. The well-suited experimental system and new methodology allowed us to study the interplay between local and systemic infection in great detail and delve into the question of how foci of primary infection interact with each other.

## MATERIALS AND METHODS

**In vitro RNA transcription and inoculation.** An infectious plasmid containing the TEV genome (GenBank accession number DQ986288) with green fluorescent protein (GFP) inserted between P1 and HC-Pro cistrons, pMTEV-GFP (36), was generously gifted by J. A. Daròs. The plasmid was linearized with BglII and transcribed into 5′-capped RNAs using the SP6 mMESSAGE mMACHINE kit (Ambion Inc.). Transcripts were precipitated (1.5 volumes of diethyl pyrocarbonate [DEPC]-treated water, 1.5 volumes of 7.5 M LiCl, 50 mM EDTA), collected, and resuspended in DEPC-treated water (4). RNA integrity was assessed by gel electrophoresis and concentration was determined spectrophotometrically using a Biophotometer (Eppendorf). *Nicotiana tabacum* L. cv. Xanthi plants were used for all experiments, and plants were maintained in a greenhouse at 25°C and with 16 h of light at all times. Four-week-old plants were mechanically inoculated on the third true leaf with 5 to 8 μg of RNA. Infected tissues were collected 7 days postinoculation (dpi) and stored at −80°C.

**Effects of $N_e$ and time of removal of the inoculated leaf on whether systemic infection is established.** Concentrated sap was obtained by grinding 500 mg of infected tissue in a mortar with 800 μl of grinding buffer (50 mM potassium phosphate [pH 7.0], 3% polyethylene glycol 6000). Then 1:3, 1:9, 1:81, 1:279, 1:500, 1:750, 1:1,000, 1:1,500, and 1:2,000 dilutions were made. We inoculated 40 4-week-old plants by abrasion of the third true leaf with 15 μl of every dilution, undiluted sap, and grinding buffer only. For each dilution, the inoculated leaf of 10 plants was removed at 40, 44, 46, 50, and 54 hours postinoculation (hpi). GFP fluorescence was observed with a Leica MZ16F stereomicroscope, using a 0.5× objective lens, and a GFP2 filter (Leica) was used to count foci of primary infection in the inoculated leaf of each dilution.

**Effects of $N_e$ and time of removal of the inoculated leaf on the number of infected cells in systemic tissues.** Thirty 4-week-old plants were inoculated by abrasion of the third true leaf with 15 μl of a 1:1 or 1:1,000 dilution of infectious TEV-GFP sap. The inoculated leaf of eight selected plants (four with 1 or 2 foci and four with approximately 100 foci) for each time point was removed at 44, 48, 54, and 100 hpi. For each plant, the first systemically infected leaf (fifth or sixth true leaf), as determined by the occurrence of TEV symptoms at 7 dpi, was analyzed. These leaves were not fully expanded, as they were harvested from 5-week-old plants. The complete leaf was harvested 7 dpi, and protoplast extraction was performed (30). Leaves were sliced thinly and incubated with enzymatic solution (0.04% cellulase and 0.015% pectinase from Sigma at 4.3 g/liter, and mannitol at 0.6 M [pH 5.8]) in the dark at 22 ± 2°C for 14 h. The solution containing protoplasts was then filtered and centrifuged (4 min at 700 rpm). Protoplasts were then purified by means of a sucrose gradient (21% sucrose, MS), washed (10 mM HEPES, 5 mM $CaCl_2$, 150 mM NaCl, 0.5 M mannitol [pH 7]), and conserved in a hormone solution (MS at 4.3 g/liter, 0.5 M mannitol [pH 5.8], hormones 1-napthaleneacetic acid [1 mg/liter], and 6-benzylaminopurine at 0.1 mg/liter).

Analysis of protoplast was carried out by flow cytometry with a Cytomics FC500 (Beckman Coulter, CA), which is equipped with an argon ion laser (488 nm, 15 mW), two detectors for light scattering (forward scatter [FS] and side scatter [SS]), and five fluorescence detectors. FS is a measure of cell size, SS is used to define protoplast granularity, and the FL4 channel with a 670-nm band-pass measures chlorophyll fluorescence. A total of 50,000 protoplasts were analyzed, and the combined FS, SS, and chlorophyll data were used to identify intact protoplasts. For intact protoplasts, GFP content was then measured on the 525-nm channel (FL1) for each individual cell.

**Effects of $N_e$ on the number of infected cells in systemic tissues.** Eight 4-week-old plants were inoculated by abrasion of the third true leaf with 15 μl of each with six different dilutions of TEV-GFP infectious sap (1:1, 1:81, 1:500, 1:1,000, 1:1,500, and 1:2,000). The inoculated leaf was then cut off the plant at 54 hpi, and foci of primary infection were counted as described previously. Isolation and analysis of protoplast were carried out by flow cytometry on the fifth or sixth true leaf at 7 dpi as described above.

**Statistical analysis.** To analyze the relationship between virion dilution and the number of primary infection foci, a factor $z\,[\ln(10^{-3}) + 3]$ is added to the ln-transformed inverse of virion dilution. This results in a "dose" that is biologically meaningful and convenient for model fitting (i.e., the maximum probability of infection is one, meaning a minimum

number of virions is needed). The number of foci plus 1 was ln transformed, because there are some uninfected plants at low doses. We then fitted a model with a dose-independent probability of infection, $N_e = pn$, and a dose-dependent probability of infection, $N_e = pn^k$, where $p$ is the infection probability, $n$ is the dose, and $k$ is a constant determining dose dependence. The models were fitted by nonlinear regression (SPSS 20.0), negative log likelihood (NLL) was calculated from the residual sum of squares (RSS) (21), and Akaike's information criteria (AIC) were used for model selection.

A generalized linear model (SPSS 20.0) was used to analyze the effects of $t_x$ (see below) and $N_e$ on the occurrence of systemic infection. The data were assumed to follow a binomial distribution, and a logit link function was used.

**Model development and model fitting.** To understand how the number of primary infection foci affects the time until the virus first establishes systemic infection ($t_{sys}$), we developed a simple dynamic model of infection. The number of primary infection foci is equivalent to the number of primary infection sites, as well as being a good estimate of $N_e$ (36). We refer to the time when the inoculated leaf was removed from the plant, always given as hours postinfection (hpi), as $t_x$. To model the transition to systemic infection, we assume that the probability that a primary infection focus will release virions that contribute to systemic infection follows a normal distribution with a mean of $\mu_t$ hours and a standard deviation $\sigma_t$. A realization from this distribution is called $t_M$, and for each focus one realization of $\mu_t$ is valid. To allow the probability that a focus causes systemic infection at a particular time point to be dependent on $N_e$, the actual size of the population contributing to systemic infection ($\eta$) is

$$\eta = N_e^{\kappa} \quad (1)$$

Here, $\kappa$ is a constant that determines whether IA, ADA (antagonistic dependent action), or SDA (synergistic dependent action) occurs. For IA, $\kappa = 1$ and the equation collapses to $\eta = N_e$. For ADA, $\kappa < 1$ and therefore the population contributing to systemic infection is smaller than $N_e$. For SDA, $\kappa > 1$ and the population contributing to systemic infection is larger than $N_e$. To model an inoculated plant, we must generate $\eta$ realizations from a normal distribution to obtain $t_M$ values. The smallest value of $t_M$ for a plant is $t_{sys}$ for that plant. We fitted our model to the experimental data using R 2.14.2 (The R Foundation, Vienna, Austria), using grid searches to estimate parameters $\mu_t$, $\sigma_t$, and $\kappa$. Model predictions and data were compared using binomial likelihoods, and we compared the fit of the IA model to the DA model using AIC.

To predict the number of infected cells in systemically infected tissues, we extended our model for $t_{sys}$. We assume that the flux of virions from each primary infection focus in the inoculated leaf, $\Phi$ virions per hour, is (i) constant over time after having started at $t_M$ and (ii) constant over all foci in the inoculated leaf. However, the actual size of the population contributing to systemic infection ($\eta$) can again be modulated when $\kappa \neq 1$ (equation 1), resulting in ADA or SDA. Note that $\kappa$ has a profound effect here, as $\eta$ modulates the cumulative virion flux for all foci of primary infection in the inoculated leaf. Note that if (i) secondary infections (i.e., any infection not in the foci of primary infection in the inoculated leaf) contribute significantly to the number of infected cells in systemic tissue and (ii) the number of cells contributing virions to systemic infection increases geometrically, we expect $\kappa$ to be >1 because the virion flux will be greater than for a linear relation with $N_e$. Nevertheless, we do not expect ADA *a priori* because we are considering events early in infection. Given that each primary infection focus produces virions from $t_M$ until $t_x$, the cumulative number of hours that foci in the inoculated leaf are releasing virions ($\lambda$) is then

$$\lambda = \sum_{t_x \geq t_M}^{\eta} (t_x - t_M) \quad (2)$$

Given that $C$ cells can be infected systemically in each plant with a probability of infection $\rho$, which is constant over plants and independent of $\lambda$, the number of infecting virions per cell will follow a Poisson distribution with a mean $\lambda\Phi\rho/C$. We simplify the model such that $\psi = \Phi\rho/C$, since we do not have good estimates of any of these parameters and our model would otherwise be overparameterized. Finally, we assume that the virus, irrespective of time, can only infect a fraction of cells $\alpha$ in the systemic tissue. This assumption is supported by the fact that we always see a considerable fraction of uninfected cells during flow cytometry (see Results and Discussion), perhaps representing cells that are largely inaccessible by means of the vascular tissue or which have had sufficient time to mount an effective immune response. Hence, we can state that proportion of infected cells in the systemically infected tissues, $I$, is equal to

$$I = \alpha(1 - e^{-\psi\lambda}) \quad (3)$$

We then fitted our model to the experimental data using grid searches to estimate parameters $\kappa$, $\Psi$, and $\alpha$, using estimates for $\mu_t$ and $\sigma_t$ from our fitted model for time of egress from the inoculated leaf. NLLs were calculated from the RSS (21) yielded by the comparison of model predictions and the experimental values of $I$, and the support for IA and DA models was determined by AIC.

## RESULTS AND DISCUSSION

**Cumulative yet independent action of primary infection foci in establishing systemic infection.** We first wanted to know how the number of primary infection foci affects the time until the virus had egressed from the inoculated leaf and first establishes systemic infection ($t_{sys}$). For our experiments, we inoculated *N. tabacum* plants with different dilutions of sap of a TEV variant expressing GFP, TEV-GFP (36). Plants were rub inoculated with different dilutions of TEV-GFP sap. The number of primary infection foci was counted by observing green fluorescence 2 days postinoculation (dpi), rendering a good estimate of the number of primary infection sites and $N_e$ (36). The inoculated leaf was then cut off the plant at $t_x$ hpi; plants were subsequently kept a further 14 days, and infection status was determined by checking for TEV symptoms. TEV symptoms are a reliable indicator, as they always appear in TEV-infected *N. tabacum* plants after approximately 1 week (37). A strong correlation between dilution and number of foci was observed in our experiments (Fig. 1), although a model with dose-dependent probability of infection per virion is better supported than a dose-independent model (Table 1). This clash with previous results (36, 37) is probably due to the much higher doses used in this study. The tapering off of the increase in focus number at higher doses suggests that it is mainly higher doses that lead to poor fit of the dose-independent-action model (Fig. 1), in agreement with previous studies on local lesions (14).

To model $t_{sys}$, we considered three scenarios: independent action (IA) and two forms of DA (dependent action), i.e., ADA (antagonistic dependent action) and SDA (synergistic dependent action). For IA, each primary infection focus has a probability of commencing the release of virions that egress the inoculated leaf and thereby cause systemic infection that follows a normal probability density function (PDF) over time. The probability of causing systemic infection at any time point is independent of $N_e$; i.e., it does not matter how many foci there are on the inoculated leaf: the PDF for initiating systemic infection over time remains the same for each focus. Moreover, as we assume that the release of virions from any one focus will be sufficient to provoke systemic infection, $t_{sys}$ occurs when the first focus releases virions. Therefore, the more foci there are in the inoculated leaf, the higher the probability that one of these foci will have started systemic infection by a given time. Therefore, $t_{sys}$ is determined by the cumulative effect of all foci, while each focus continues to act independently (Fig. 2). We consider IA the null model.

For ADA, as the number of primary infection foci increases,

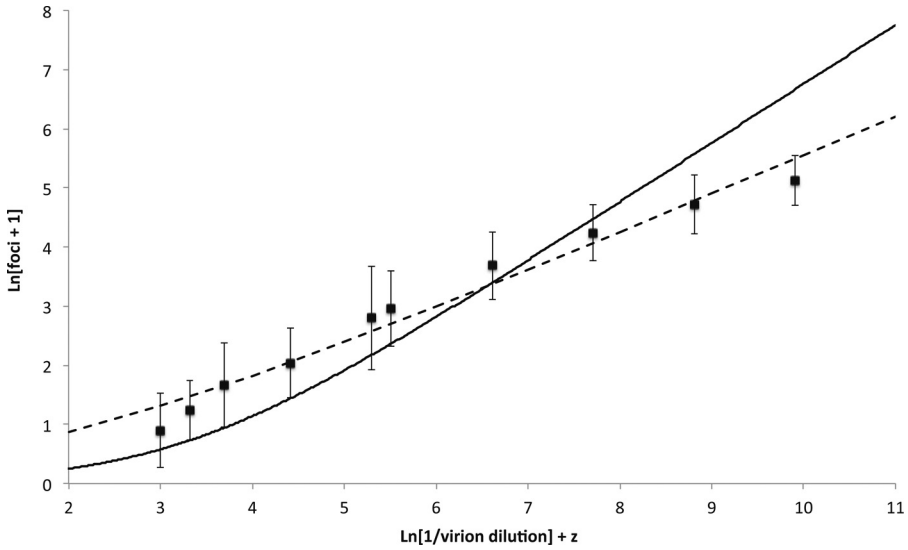


**FIG 1** Relationship of dose to primary infection foci. On the abscissa is the ln-transformed inverse of the virion dilution, which is equivalent to dose on an arbitrary scale, while on the ordinate is the ln-transformed number of foci (see Materials and Methods). Squares represent the experimental data, with error bars indicating the standard deviations. The continuous line represents a fitted dose-independent-action model, whereas the dotted line represents a dose-dependent-action model (see Materials and Methods). The dose-dependent-action model was better supported (Table 1), indicating that the probability of infection decreases with dose. Note that for the dose-independent action model, altering the probability of infection ($p$) will only shift the position of the response to the right or left and not change its shape on a logarithmic scale. For the experimental data, at higher doses the increase in the focus number with dose appears to taper off, suggesting that it is mainly the higher doses that deviate from dose-independent model predictions; i.e., the dose-independent-action response could be reasonably fitted to only the low-dose data (ln[dose] $< 6$) by increasing $p$ and thereby shifting the response to the left, whereas given its fixed shape the model cannot be fitted well to the high-dose data (ln[dose] $> 6$). This effect might occur because the number of infectious sites in the inoculated leaf becomes saturated at high doses.

the probability that any one focus will cause systemic infection at a particular time point decreases. Therefore, the effect of an increase in $N_e$ on $t_{sys}$ is weaker for the ADA model than for the IA model (Fig. 3A and B). One probable mechanism for ADA would be that different foci constrain each other's spatial radiation and hereby hinder each other's access to vascular tissue (7, 36). Given that foci of primary infection expand in a largely two-dimensional surface (i.e., the inoculated leaf), such hindrances could conceivably be important to infection dynamics. For SDA, as the number of primary infection foci increases, the probability that any one focus will cause systemic infection at a particular time point increases. Therefore, the effect of an increase in $N_e$ on $t_{sys}$ is stronger for the SDA model than for the IA model (Fig. 3B and C). SDA occurs if many sites of primary infection could overwhelm the host immune system, expediting the onset of systemic infection. We do not consider SDA very likely *a priori* but allow for the possibility in our modeling nonetheless. The key parameter for the DA model is $\kappa$. When $\kappa = 1$, the model collapses to the IA model (Fig. 3B). For ADA, $\kappa < 1$, and therefore the population contributing to systemic infection is smaller than $N_e$ (Fig. 3A). For SDA, $\kappa > 1$, and the population contributing to systemic infection is larger than $N_e$ (Fig. 3C). As the difference between ADA and SDA depends only on a parameter value, we subsequently refer to this model as the DA model. Both models were fitted to the data by a maximum likelihood-based method, and model selection was done by means of the Akaike information criterion (AIC).

**TABLE 1** Estimated model parameters for the fitting of the relationship of dose versus primary infection foci[a]

| Model | $p$ | $k$ | NLL | AIC | ΔAIC | AW |
|---|---|---|---|---|---|---|
| Dose-dependent $p$ | 0.384 ± 0.037 | 0.650 ± 0.014 | 286.2 | 576.4 | | 1.000 |
| Dose-independent $p$ | 0.039 ± 0.002 | | 1913.4 | 3828.8 | 3252.5 | 0.000 |

[a] Fitting of a dose-independent and dose-dependent probability of infection models to the relationship of dose versus primary infection foci (Fig. 1). The parameter $p$ is the probability of infection, while the parameter $k$ in effect modifies the probability of infection for the dose-dependent model. The dose-dependent model is clearly better supported, indicating that the probability of infection in effect decreases with dose as $k < 0$. ΔAIC, difference in AIC with the best-fitting model; AW, Akaike weight.

For the experimental data, the occurrence of systemic infection appears to be dependent on both $t_x$ and $N_e$ (Fig. 4). For low values of $t_x$ (40 hpi), there were few infected plants for $N_e$ values below 100, whereas for high values of $t_x$ (54 hpi), an uninfected plant was observed only for the lowest $N_e$ value used. At intermediate $t_x$ values, the occurrence of systemic infection appears to increase as $N_e$ is increased. Statistical analysis of the experimental data clearly shows that infection status of the plant was dependent on both $t_x$ and $N_e$ ($P < 0.001$), and there was a significant positive interaction ($P < 0.001$) (generalized linear model; see Materials and Methods). Negative log likelihood (NLL) values indicated that both the IA and DA models fitted the data equally well, favoring the more parsimonious IA model in the model selection (Table 2). Moreover, for the DA model a $\kappa$ value of 0.99 was estimated, further reinforcing the idea that the IA model best describes the data. The conclusions supported by model fitting are concurrent with the statistical analysis, given that the DA model predicts effects of $N_e$ and $t_x$, and an interaction between these two variables.

We therefore conclude that the data support the idea that the cumulative effect of independently acting foci of primary infection determines when the plant first becomes systemically infected. We were surprised by this result, since the largely two-dimensional structure of the leaf could conceivably cause

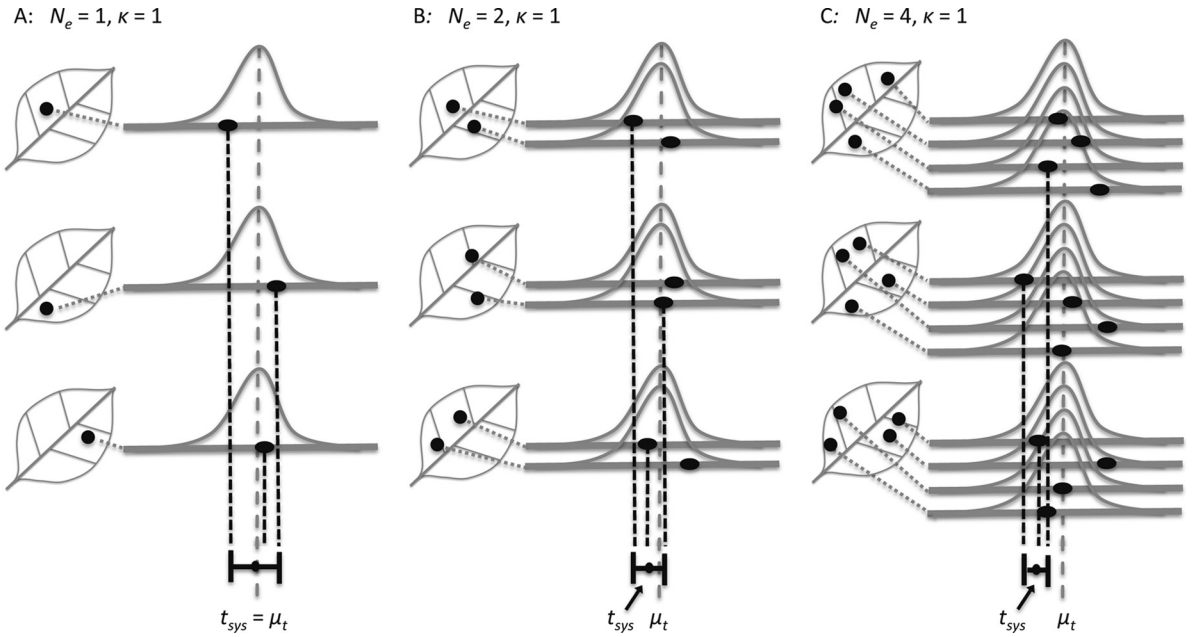


**FIG 2** Conceptual model of viral egress from the inoculated leaf. We illustrate conceptually our null model of the infection process—independent action (IA). Black dots on the leaf indicate primary infection foci. The gray bell-shaped curves are the PDF for egress from the inoculated leaf over time for individual foci, with time increasing from left to right and a mean $\mu_t$. The black dot on the curve indicates $t_M$, one realization of $\mu_t$ (i.e., drawing a value from the PDF) for each focus. Systemic infection commences at $t_{sys}$ when the first focus generates virions that egress the inoculated leaf. As the number of foci per inoculated leaf increases from 1 (A) to 2 (B) to 4 (C), $t_{sys}$ occurs faster due to the cumulative action of independently acting foci, because as the number of realizations increases, the probability of drawing a shorter time increases. We could also expect the distribution of $t_{sys}$ to become skewed toward low values as the number of primary infection foci increases: the fastest draw determines $t_{sys}$, and one must therefore draw only slow values to obtain $t_{sys}$.

interference between primary infection foci (7, 36). Our modeling results do not, however, necessarily imply that there is no interference between primary infection foci; rather, they imply that we do not need to invoke interference to describe empirically observed patterns. We think that some interference is likely to occur when the number of primary infection foci is high. However, we speculate that the effects thereof will be largely invisible given that $t_{sys}$ will already be attenuated at the $N_e$ values necessary for interference, because of the exact dimensions of the distribution of first virion release of primary infection foci over time ($\mu_t$ and $\sigma_t$).

**Cumulative yet independent action determines the proportion of virus-infected cells in systemic tissue.** The IA model was supported when the establishment of systemic infection was considered dichotomously (i.e., whether plants were systemically infected or not). However, to better understand this experimental system and subject IA to a more stringent test, we also sought to compare model predictions to quantitative measurements of an infection parameter. We therefore measured the number of TEV-infected cells in systemically infected tissue while varying $t_x$ and $N_e$. These measurements were performed by isolating protoplasts

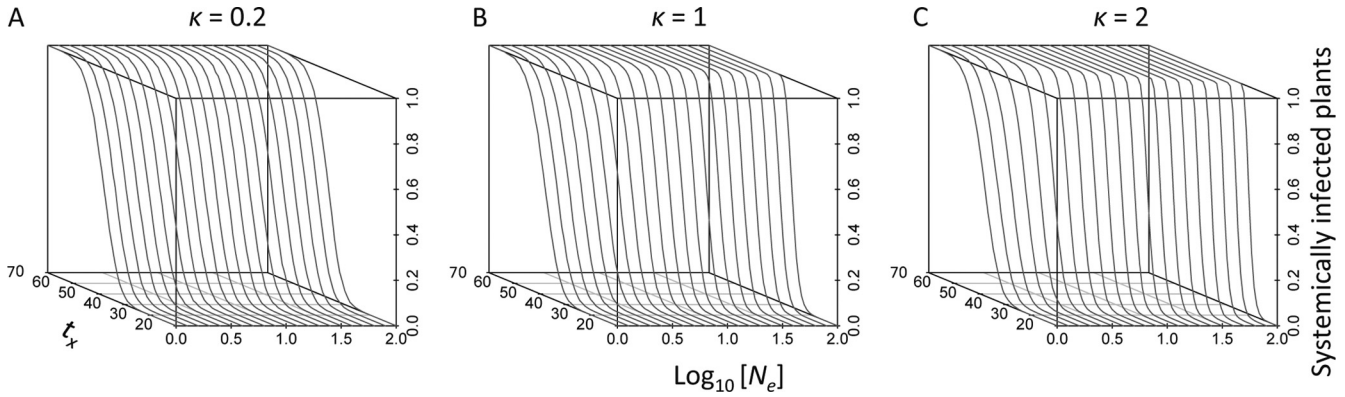


**FIG 3** Model predictions for viral egress from the inoculated leaf. The relation between effective population size ($N_e$), the time of removal of the inoculated leaf ($t_x$), and the time when the plant becomes systemically infected ($t_{sys}$) predicted by our model is given. For all three panels, log-transformed $N_e$ is on the *x* axis, $t_x$ is on the *y* axis, and the frequency of systemic infection is given on the *z* axis. If $\kappa < 1$ (ADA [A]), $t_{sys}$ decreases slower as $N_e$ increases than for the IA model ($\kappa = 1$ [B]). If $\kappa > 1$ (SDA [C]), $t_{sys}$ decreases faster as $N_e$ increases than for the IA model, resulting in ADA. Note that for $N_e = 1$, the distribution of the frequencies is the same in all three panels and equivalent to the distribution of $t_{sys}$ for a single primary infection focus.

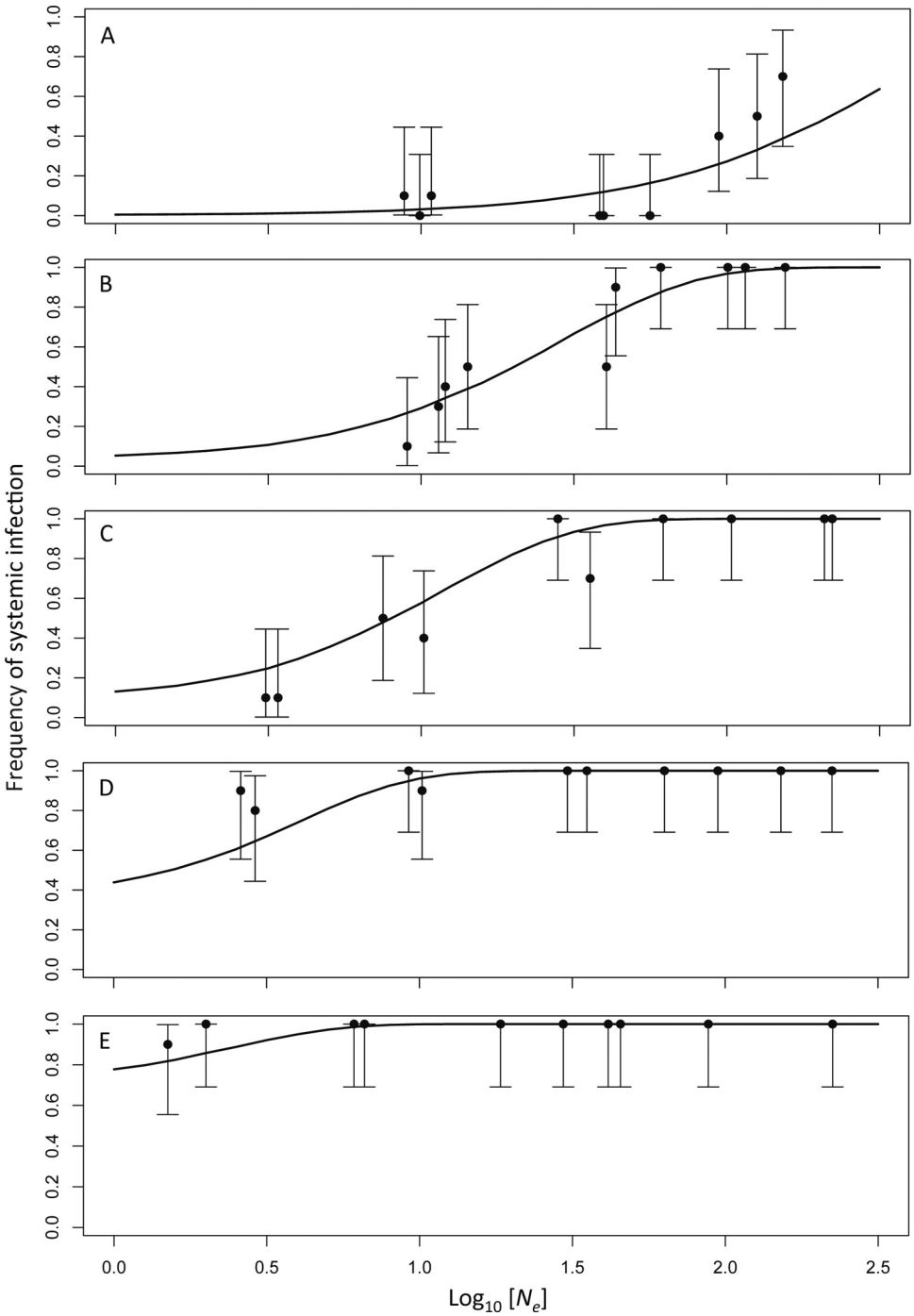


**FIG 4** Systemic infection when the inoculated leaf is removed at different times. Plants were rub inoculated, and the inoculated leaf was removed at a given number of hours postinoculation ($t_x$). The relation between log $N_e$ (abscissa) and the frequency of systemic infection (ordinate) was plotted here, when the inoculated leaf was removed after 40 h (A), 44 h (B), 46 h (C), 50 h (D), and 54 h (E). Error bars indicate 95% confidence intervals. The lines represent the fitted independent-action (IA) model (Table 1), which was fitted simultaneously to all the data represented here. The frequency of systemic infection increases with $N_e$ and $t_x$.

from the first systemically infected leaf (the fifth or sixth true leaf) at 7 dpi (30) and using flow cytometry to determine which cells had been infected by TEV-GFP (see Materials and Methods). We could therefore accurately estimate the proportion of infected cells in the systemic tissue first targeted by the virus.

A total of 50,000 protoplasts were analyzed, and the combined FS, SS, and chlorophyll data were used to identify intact protoplasts (Fig. 5A and B). For intact protoplasts, GFP content was then measured on the 525-nm channel (FL1) for each individual cell (Fig. 5C). GFP fluorescence (FM) had a higher mean and less variation for intact protoplasts than for those protoplasts excluded from the analysis based on FS, SS, and

**TABLE 2** Estimated model parameters and AIC values for egress of the inoculated leaf[a]

| Model | $\mu_t$ | $\sigma_t$ | $\kappa$ | NLL | AIC | ΔAIC | AW |
|---|---|---|---|---|---|---|---|
| IA | 52.00 | 4.40 | | 50.646 | 105.292 | | 0.723 |
| DA | 51.85 | 4.40 | 0.99 | 50.605 | 107.210 | 1.918 | 0.277 |

[a] Estimated model parameters ($\mu_t$, $\sigma_t$, and $\kappa$; see Materials and Methods and Fig. 1) and the results of model selection for the independent-action (IA) and dependent-action (DA) models. ΔAIC, difference in AIC with the best-fitting model; AW, Akaike weight. The two models give essentially the same prediction, since when $\kappa = 1$ the DA model collapses to the IA model. AIC and AW therefore slightly favor the simpler IA model.

chlorophyll criteria (Fig. 5D). Results for our selection criteria and FM therefore suggest that there is not a continuum in cellular integrity in our population of protoplasts but, rather, a population of largely intact cells on the one hand and damaged protoplasts or debris on the other. A clear dichotomy between noninfected cells and debris is required to measure accurately the proportion of infected cells.

To model the proportion of infected cells in the systemically infected tissue, we extended the model for the time of establishment of systemic infection. We assume that the flux of virions from each primary infection focus in the inoculated leaf is the same for every focus and constant over time (Fig. 6). However, the number of foci that contribute to systemic infection can again be modulated by a constant $\kappa$, similar to the model for systemic infection establishment time. If $\kappa = 1$, the model collapses to an IA model. If $\kappa < 1$, the net effect is that virion flux per focus increases with $N_e$ (SDA), leading to a smaller increase in the number of infected cells in the systemic tissue as $N_e$ increases than for the IA model (Fig. 7A and B). Conversely, if $\kappa > 1$, virion flux increases with $N_e$, resulting in ADA (Fig. 7B and C). Here, ADA and SDA could occur for the same reasons as in the infection establishment model (7, 36). SDA-like effects could also occur if secondary infections affect the number of infected cells in systemic tissue (i.e., any infected cell outside the primary infection foci contributing to cumulative virion flux), which we consider unlikely *a priori* because we are considering events early in infection. To estimate the number of infected cells in systemic tissue, the model then only

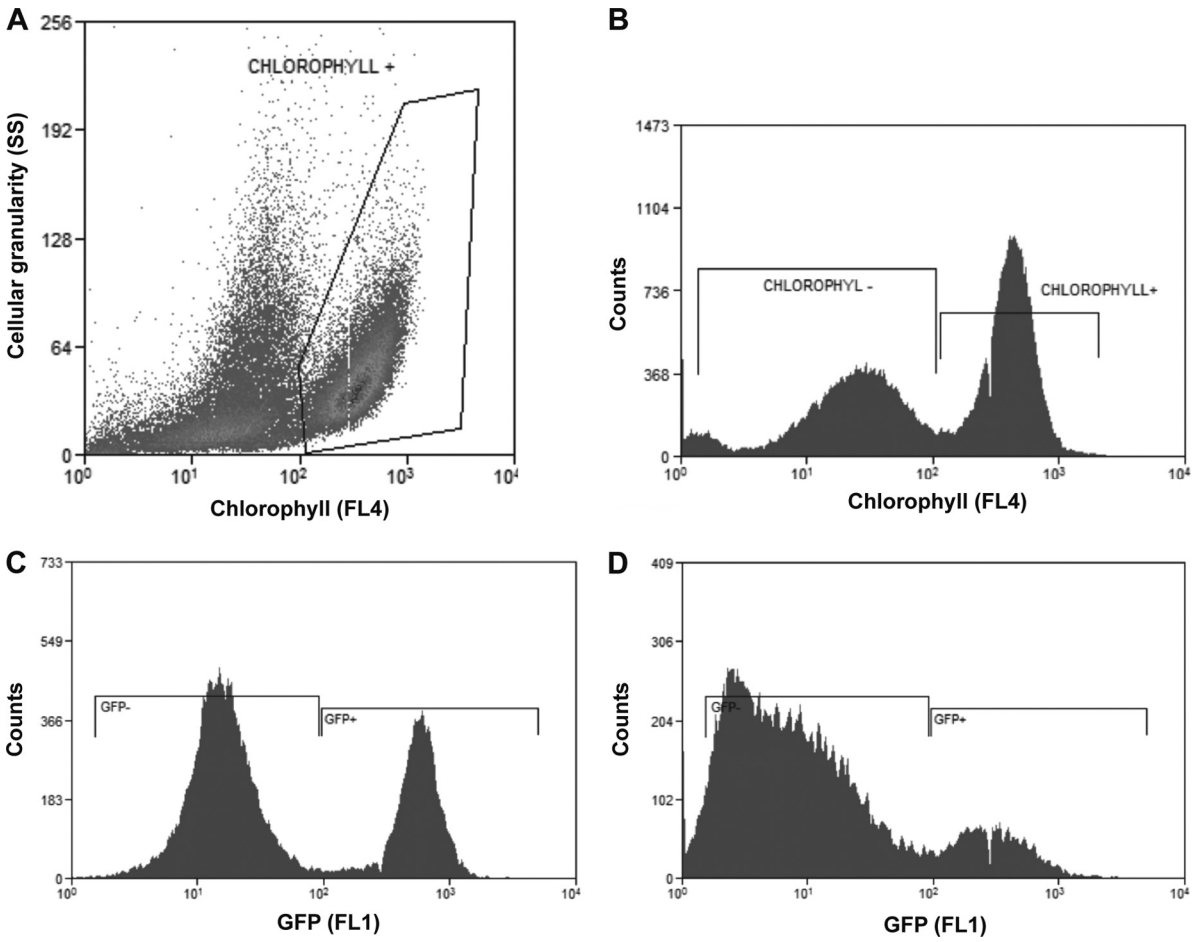


**FIG 5** Selection on intact protoplasts. In panel A, we show the selection of the intact protoplast population by plotting chlorophyll content (as measured on the FL4 channel) on the abscissa and cellular granularity (as measured by side scatter [SS]) on the ordinate. The population of protoplasts selected for further analysis is indicated by the polygon. In panel B, the discontinuity of protoplast chlorophyll content is illustrated by plotting chlorophyll signal (FL4) on the abscissa and counts on the ordinate; the data can be easily segregated into populations with high and low chlorophyll contents. The GFP signal for protoplasts (abscissa) selected for further analysis (C) and those rejected (D) is divergent in terms of cell counts (ordinate). For selected protoplasts (C), two populations with relatively low heterogeneity can be easily discriminated, with the cutoff determined by the threshold values from GFP-negative controls. For rejected protoplasts the average signal is lower, with most being in the range observed in the negative control, and more heterogeneous (D).

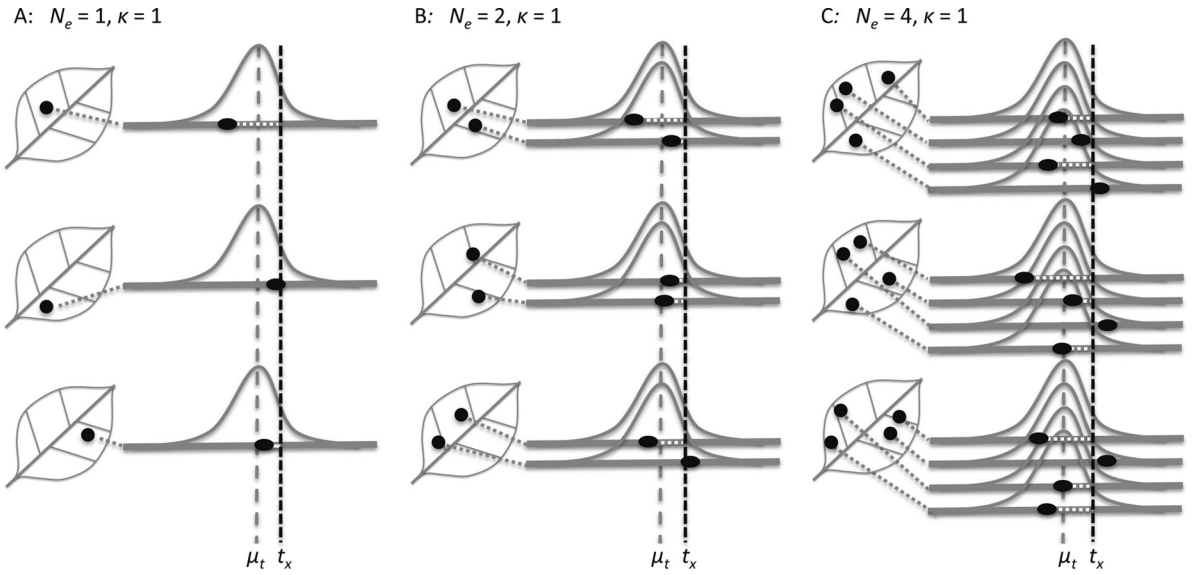


**FIG 6** Conceptual model of the proportion of infected cells in the systemic tissue. We illustrate conceptually our null model of the infection process—independent action (IA)—for predicting the number of systemically infected cells. Black dots on the leaf indicate primary infection foci. The bell-shaped curves are the PDF for egress from the inoculated leaf over time for individual foci, with time increasing from left to right. The black dot on the curves indicates $t_M$, one realization of $\mu_t$ (i.e., drawing a value from the PDF), for each focus. Each focus produces virions from $t_M$ until $t_x$, which is marked by the vertical dotted black line, and the sum of positive values obtained by subtracting $t_M$ from $t_x$ determines the total number of virions produced in the inoculated leaf (λ). As the number of foci per inoculated leaf increases from 1 (A) to 2 (B) to 4 (C), the cumulative number of virions released by the inoculated leaf increases. The infection of systemically infected cells then depends on α, the proportion of cells in the systemic tissue that are susceptible to infection, and a parameter representing the probability of infection of a cell and the number of cells available in the systemic tissue (Ψ).

requires a parameter to link the cumulative virion flux prior to the removal of the inoculated leaf to the number of infected cells (ψ), and the proportion of cells in the systemic tissue that can become infected (α).

Two experiments in which we measured the proportion of systemically infected cells by flow cytometry were performed. First, we infected plants with a low dose ($N_e \approx 1$) and a high dose ($N_e \approx 100$) and removed the inoculated leaf at different time points (Fig. 8A). Statistical analysis of the data show that $N_e$ and a positive interaction between $N_e$ and $t_x$ had a significant effect on the proportion of infected cells, whereas the effect of $t_x$ alone was not significant (Table 3). This result was therefore somewhat similar to that for the time of establishment of systemic infection (Fig. 4). This result is also intuitive: the combination of more primary infection foci and longer time before the removal of the inoculated leaf results in a greater of number of virions egressing the inoculated leaf and infecting cells in systemic tissues. The IA model was also best supported for this experiment (Table 4). Second, we inoculated plants with a range of doses, quantified $N_e$ by counting the number of primary infection foci, and removed the inoculated

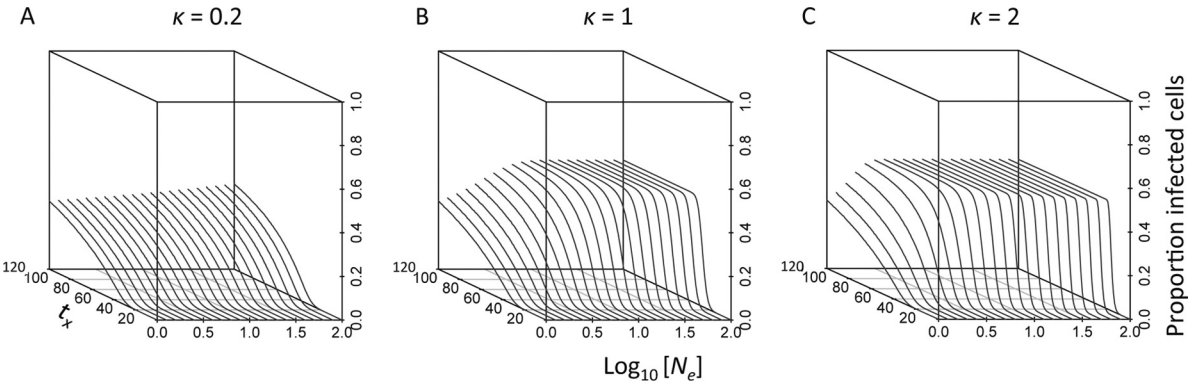


**FIG 7** Model predictions for the proportion of infected cells in the systemic tissue. The relation between effective population size ($N_e$), the time of removal of the inoculated leaf ($t_x$), and the proportion of infected cells in the systemically infected tissue ($I$) predicted by our model is given for different κ values. For all three panels, log-transformed $N_e$ is on the $x$ axis, $t_x$ is on the $y$ axis, and $I$ is on the $z$ axis. When $\kappa < 1$ (ADA [A]), $I$ increases slowly for a particular value of $N_e$ and does not completely reach saturation for large $N_e$ values. When $\kappa = 1$ (B), $I$ increases rapidly with $t_x$ as $N_e$ becomes larger. When $\kappa > 1$ (SDA [C]), the increase occurs even more quicklyand the response eventually becomes almost horizontal; the window in which $t_x$ values will lead to intermediate $I$ values (i.e., $0 > I > \alpha$) becomes very small. Note that similar to the model for $t_{sys}$, when $N_e = 1$ the $t_x$ versus $I$ relation remains the same irrespective of κ. When $N_e = 1$, $I$ can only be modulated by α, the proportion of cells which is susceptible to infection, and Ψ, a parameter linking the cumulative time that foci release virions to the number of systemically infected cells (see Materials and Methods).

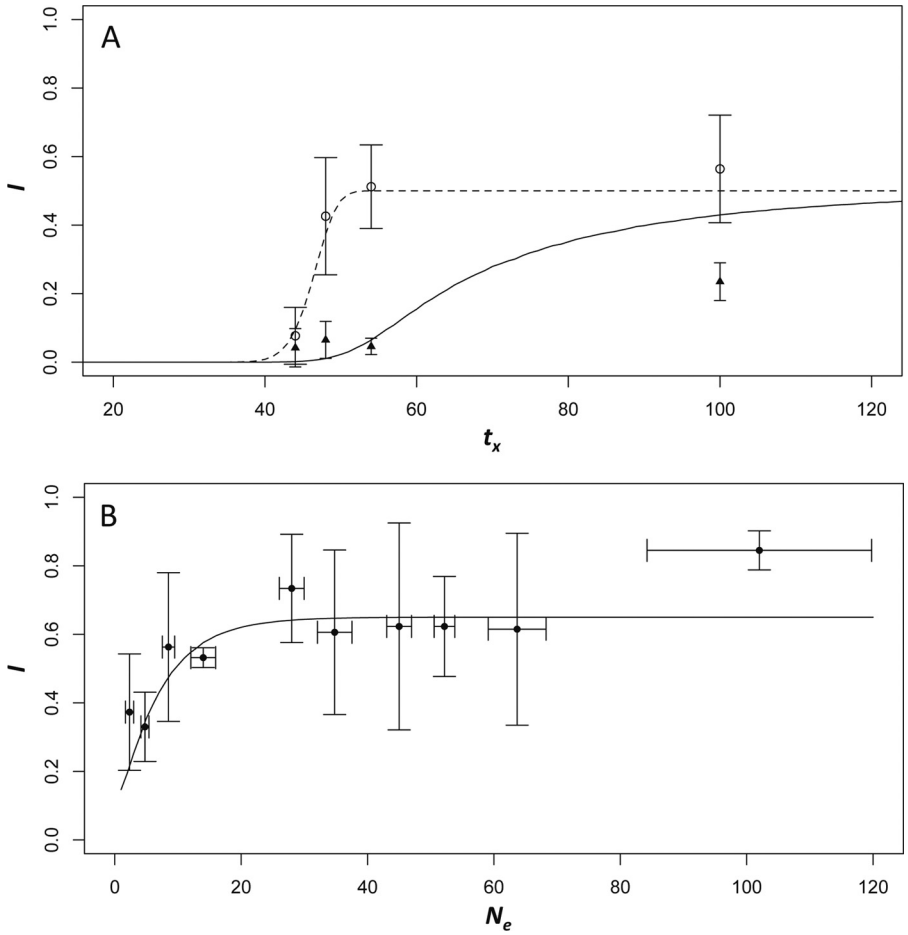


**FIG 8** Effects of $N_e$ and $t_x$ on the number of infected cells. In panel A, the experimental data fitted the IA model for the effects of the time of the removal of the inoculated leaf ($t_x$, on the abscissa) on the number of infected cells in the systemically infected tissue ($I$, on the ordinate). The solid triangles and solid line represent the data and model, respectively, for a small $N_e$ (1), while the open circles and dotted line represent a large $N_e$ (100). Error bars represent 95% confidence limits for the data. The IA model was better supported than the DA model, as indicated by AIC-based model selection (Table 4), and accounts satisfactorily for most of the data. The fitted model must account for all the data in the panel, and the only discrepancy between the data and the IA model occurs when $N_e$ is small and $t_x = 100$. In panel B, the effects of $N_e$ (abscissa) on the number of infected cells in the systemically infected tissue ($I$, on the ordinate) is shown, when the inoculated leaf was removed at the same time ($t_x = 54$ hpi) for all plants. Circles represent the experimental data, with error bars representing 95% confidence intervals, and the line represents the model. To represent the data, $N_e$ values of 1 to 3, 4 to 6, 7 to 9, 10 to 19, 20 to 29, 30 to 39, 40 to 49, 50 to 59, 60 to 69, and >70 were grouped together. The IA model was better supported than the DA model, and fitted-model parameters are similar to those of the other experiment measuring $I$ (in which $t_x$ was also varied [Table 2]).

**TABLE 3** ANOVA and variance components for $I$ data[a]

| Expt no. | Variation source | *SS* | d.f. | *MS* | *F* | *P* | Explanation of variance (%) |
|---|---|---|---|---|---|---|---|
| 1 | $t_x$ | 0.952 | 3 | 0.317 | 2.322 | 0.254 | 13.54 ± 0.39 |
| | $N_e$ | 1.418 | 1 | 1.418 | 10.377 | 0.049 | 29.58 ± 1.04 |
| | $N_e \times t_x$ | 0.410 | 3 | 0.137 | 6.139 | 0.001 | 23.05 ± 0.33 |
| | Error | 1.246 | 56 | 0.022 | | | 33.82 ± 0.03 |
| 2 | $N_e$ | 1.143 | 9 | 0.127 | 3.713 | 0.003 | 33.41 ± 0.26 |
| | Error | 1.128 | 33 | 0.034 | | | 66.59 ± 0.13 |

[a] Two-way analysis of variance (ANOVA) on the data from the experiments measuring the proportion of infected cells in systemically infected tissue when both $t_x$ and $N_e$ were varied (experiment 1; see Fig. 6), and the proportion of infected cells in the systemically infected tissue when only $N_e$ was varied (experiment 2; see Fig. 7). *SS*, sum of squares; d.f., degrees of freedom; *MS*, mean square. Explanation of variance is the percentage of variance explained by the model, which was estimated by a maximum likelihood-based variance components analysis in SPSS, and the asymptotic covariance is given as an indication of estimate error.

leaf at 54 hpi for all plants (Fig. 8B). The proportion of infected cells was then significantly dependent on $N_e$ (Table 3), and the IA model was once again best supported (Table 4). Therefore, we conclude that $N_e$-dependent effects do not need to be invoked to understand the proportion of systemically infected cells.

The data and fitted model both suggest that when $N_e$ is large ($N_e \approx 100$), the maximum number of infected cells in the systemic tissue of the plant is reached rapidly (Fig. 8A). However, even when $N_e$ is small ($N_e \approx 1$), the number of systemically infected cells eventually can reach levels similar to those for large $N_e$ values (Fig. 7 and 8). These observations also help to explain why there are only $N_e$-dependent effects on viral accumulation if the inoculated leaf is removed upon first sign of systemic infection, and why there are no effects if the inoculated leaf is not removed (37). Moreover, we speculate that similar to the establishment of systemic infection, there will be antagonistic $N_e$-dependent effects on the flux of virions from the inoculated leaf when $N_e$ values are

**TABLE 4** Estimated model parameters and AIC values for the number of infected cells[a]

| Expt. no. | Model | κ | Ψ | α | NLL | AIC | ΔAIC | AW |
|---|---|---|---|---|---|---|---|---|
| 1 | IA | | $2.5 \times 10^{-2}$ | 0.52 | 8.685 | 21.370 | | 0.640 |
| | DA | 1.22 | $1.0 \times 10^{-2}$ | 0.55 | 8.262 | 22.524 | 1.154 | 0.360 |
| 2 | IA | | $6.3 \times 10^{-2}$ | 0.70 | 6.336 | 16.672 | | 0.707 |
| | DA | 0.84 | $1.0 \times 10^{-1}$ | 0.65 | 6.219 | 18.438 | 1.766 | 0.293 |

[a] Estimated model parameters (κ, ψ, and α; see Materials and Methods and Fig. 4) and the results of model selection for the independent-action (IA) and dependent-action (DA) models for two experiments. For experiment 1, $N_e$ and $t_x$ were both varied (Fig. 6), while for experiment 2, only $N_e$ was varied (Fig. 7). ΔAIC, difference in AIC with the best-fitting model; AW, Akaike weight. NLL values demonstrate that for both experiments the fit of the alternative model (DA) is slightly better than that of the null model (IA), but AIC values show that this improved fit does not justify the addition of the extra model parameter (κ). Hence, the IA model is best supported for both experiments.

large. However, we expect that the number of infected cells in systemic tissue will be saturated by the virion production of only a small number of foci, and hence these effects will not be manifest. Finally, our observations suggest that evolution has optimized TEV for small $N_e$ values, since both viral accumulation (37) and the number of systemically infected cells saturate with small $N_e$ values, and both parameters are undoubtedly fitness components in the field.

**Concluding remarks.** We found no evidence for $N_e$-dependent interactions between primary infection foci, suggesting that the dynamics of systemic infection establishment are the result of the cumulative yet independent action of primary infection foci. These effects are analogous to buying more tickets in a fair lottery: the probability that an individual person will win a prize increases with the number of lottery tickets they buy, while the probability that any one lottery ticket is drawn and wins a prize remains the same. Similarly, having more foci of primary infection will result in an increased probability of systemic infection occurring earlier and in a greater proportion of cells in the systemically infected tissue, while the probability of achieving systemic infection and infecting a cell remains the same for each primary infection focus. Of course, there may be superinfection exclusion at the cellular level (7), but since we are considering cells dichotomously (noninfected versus infected), we can ignore these types of effects for modeling our experimental setup. Thus, we find evidence that the IA model of infection may also apply to more complex dynamic processes in infection when individuals of a conspecific pathogen population are coinoculated.

Our model assumes that the time at which primary infection foci first release virions that contribute to systemic infection varies, following a normal distribution. However, what mechanisms could generate this variation? To contribute to systemic infection following mechanical inoculation, the virus must expand from the primary infected cell in the epidermis until it reaches companion cells to sieve elements by cell-to-cell movement (5, 8). Therefore, one could speculate that random variation in the number of cells the virus must traverse is probably the main mechanism generating variation in the time when foci commence contributing to systemic infection.

Although our results illustrate that independent action in establishing systemic infection is a viable hypothesis, we think this result is best seen as a proof of principle. First, infection dynamics are likely to be more complex for multipartite viruses which encapsidate genome segments in different virion or movement-complex types. If complementation between independently transmitted genome segments is necessary, then we would expect synergistic interactions between foci especially with respect to the number of systemically infected cells. Second, viruses that immediately access vascular tissue upon inoculation (i.e., without replication) will be subject to different infection dynamics, in which dispersion of virions probably plays a key role early in infection. For example, *Beet curly top virus*, a phloem-limited virus (34), egressed from the inoculated leaf and traversed petioles of up to 17.78 cm within 30 min of exposure to viruliferous vectors (31). Third, the combination of TEV and tobacco is in some respects unusual; the probability that a primary infection focus causes systemic infection is practically 1, and there does not appear to be a strong genetic bottleneck during the colonization of systemically infected leaves (36, 37). Although *Cauliflower mosaic virus* infection can be similar to TEV in this respect (27), other viruses clearly show different infection dynamics (18, 19, 25, 29). Fourth, our results suggest that the systemic tissue of the plant can be largely saturated by virion production of a small number of primary infection foci. If this is not the case in a particular pathosystem, we think that antagonistic $N_e$-dependent interactions are more likely to contribute manifestly to the observed dynamics. Finally, if the host is able to mount an effective immune response on short time scales, antagonistic $N_e$-dependent interactions would also be more likely to occur. We speculate that this will be the case in many other pathosystems with readily primed immune mechanisms, such as the formation of local lesions (2) and other hypersensitivity responses, sloughing of target tissues for primary infection (11, 20), or rapid deployment of phagocytes. Nevertheless, we show that IA cannot be discarded *a priori* for description of infection dynamics, even in a complex multicellular host with an effective immune system and heterogeneous spatial organization.

## ACKNOWLEDGMENTS

We thank Francisca de la Iglesia and Alicia Martínez for technical support.

This research was supported by grants from the Spanish Ministerio de Economía y Competitividad, BFU2009-06993 to S.F.E. and a "Juan de la Cierva" postdoctoral contract (JCI-2011-10379) to M.P.Z.

## REFERENCES

1. **Ali A, et al.** 2006. Analysis of genetic bottlenecks during horizontal transmission of *Cucumber mosaic virus*. J. Virol. **80**:8345–8350.
2. **Bald JG.** 1937. The use of numbers of infections for comparing the concentration of plant virus suspensions. I. Dilution experiments with purified suspensions. Ann. Appl. Biol. **24**:33–55.
3. **Betancourt M, Fereres A, Fraile A, García-Arenal F.** 2008. Estimation of the effective number of founders that initiate an infection after aphid transmission of a multipartite plant virus. J. Virol. **82**:12416–12421.
4. **Carrasco P, Daròs JA, Agudelo-Romero P, Elena SF.** 2007. A real-time RT-PCR assay for quantifying the fitness of *Tobacco etch virus* in competition experiments. J. Virol. Methods **139**:181–188.
5. **Carrington JC, Kasschau KD, Mahajan SK, Schaad MC.** 1996. Cell-to-cell and long-distance transport of viruses in plants. Plant Cell **8**:1669–1681.
6. **Cheng NH, Su CL, Carter SA, Nelson RS.** 2000. Vascular invasion routes and systemic accumulation patterns of *Tobacco mosaic virus* in *Nicotiana benthamiana*. Plant J. **23**:349–362.
7. **Dietrich C, Maiss E.** 2003. Fluorescent labelling reveals spatial separation of *Potyvirus* populations in mixed infected *Nicotiana benthamiana* plants. J. Gen. Virol. **84**:2871–2876.
8. **Ding XS, Shintaku MH, Carter SA, Nelson RS.** 1996. Invasion of minor

veins of tobacco leaves inoculated with *Tobacco mosaic virus* mutants defective in phloem-dependent movement. Proc. Natl. Acad. Sci. U. S. A. **93**:11155–11160.
9. **Druett HA.** 1952. Bacterial invasion. Nature **170**:288.
10. **Engelhard EK, Kammorgan LNW, Washburn JO, Volkman LE.** 1994. The insect tracheal system—a conduit for the systemic spread of *Autographa californica* M nuclear polyhedrosis virus. Proc. Natl. Acad. Sci. U. S. A. **91**:3224–3227.
11. **Engelhard EK, Volkman LE.** 1995. Developmental resistance in 4th-instar *Trichoplusia ni* orally inoculated with *Autographa californica* M nuclear polyhedrosis virus. Virology **209**:384–389.
12. **Fabre F, et al.** 2012. Modelling the evolutionary dynamics of viruses within their hosts: a case study using high-throughput sequencing. PLoS Pathog. **8**:e1002654. doi:10.1371/journal.ppat.1002654.
13. **French R, Stenger DC.** 2003. Evolution of *Wheat streak mosaic virus*: dynamics of population growth within plants may explain limited variation. Annu. Rev. Phytopathol. **41**:199–214.
14. **Furumoto WA, Mickey R.** 1967. A mathematical model for infectivity-dilution curve of *Tobacco mosiac virus*-experimental tests. Virology **32**: 224–233.
15. **Gillespie T, et al.** 2002. Functional analysis of a DNA-shuffled movement protein reveals that microtubules are dispensable for the cell-to-cell movement of *Tobacco mosaic virus*. Plant Cell **14**:1207–1222.
16. **González-Jara P, Fraile A, Canto T, García-Arenal F.** 2009. The multiplicity of infection of a plant virus varies during colonization of its eukaryotic host. J. Virol. **83**:7487–7494.
17. **Gutiérrez S, et al.** 2010. Dynamics of the multiplicity of cellular infection in a plant virus. PLoS Pathog. **6**:e1001113. doi:10.1371/journal.ppat.1001113.
18. **Hall JS, French R, Hein GL, Morris TJ, Stenger DC.** 2001. Three distinct mechanisms facilitate genetic isolation of sympatric *Wheat streak mosaic virus* lineages. Virology **282**:230–236.
19. **Hall JS, French R, Morris TJ, Stenger DC.** 2001. Structure and temporal dynamics of populations within *Wheat streak mosaic virus* isolates. J. Virol. **75**:10231–10243.
20. **Herrero S, et al.** 2007. REPAT, a new family of proteins induced by bacterial toxins and baculovirus infection in *Spodoptera exigua*. Insect Biochem. Mol. Biol. **37**:1109–1118.
21. **Johnson JB, Omland KS.** 2004. Model selection in ecology and evolution. Trends Ecol. Evol. **19**:101–108.
22. **Kleczkowski A.** 1950. Interpreting relationships between the concentrations of plant viruses and numbers of local lesions. J. Gen. Microbiol. **4**:53–69.
23. **Kuss SK, Etheredge CA, Pfeiffer JK.** 2008. Multiple host barriers restrict poliovirus trafficking in mice. PLoS Pathog. **4**:e1000082. doi:10.1371/journal.ppat.1000082.
24. **Leisner SM, Turgeon R, Howell SH.** 1993. Effects of host plant development and genetic determinants on the long-distance movement of *Cauliflower mosaic virus* in *Arabidopsis*. Plant Cell **5**:191–202.
25. **Li HY, Roossinck MJ.** 2004. Genetic bottlenecks reduce population variation in an experimental RNA virus population. J. Virol. **78**:10582–10587.
26. **Miyashita S, Kishino H.** 2010. Estimation of the size of genetic bottlenecks in cell-to-cell movement of *Soil-borne wheat mosaic* virus and the possible role of the bottlenecks in speeding up selection of variations in *trans*-acting genes or elements. J. Virol. **84**:1828–1837.
27. **Monsion B, Froissart R, Michalakis Y, Blanc S.** 2008. Large bottleneck size in *Cauliflower mosaic virus* populations during host plant colonization. PLoS Pathog. **4**:e1000174. doi:10.1371/journal.ppat.1000174.
28. **Moury B, Fabre F, Senoussi R.** 2007. Estimation of the number of virus particles transmitted by an insect vector. Proc. Natl. Acad. Sci. U. S. A. **104**:17891–17896.
29. **Sacristán S, Malpica JM, Fraile A, García-Arenal F.** 2003. Estimation of population bottlenecks during systemic movement of *Tobacco mosaic virus* in tobacco plants. J. Virol. **77**:9906–9911.
30. **Sankara Rao K, Prakash AH.** 1995. A simple method for the isolation of plant protoplasts. J. Biosci. **20**:645–655.
31. **Severin HHP.** 1924. Curly leaf transmission experiments. Phytopathology **14**:80–93.
32. **Smith DR, Adams AP, Kenney JL, Wang E, Weaver SC.** 2008. *Venezuelan equine encephalitis virus* in the mosquito vector *Aedes taeniorhynchus*: infection initiated by a small number of susceptible epithelial cells and a population bottleneck. Virology **372**:176–186.
33. **Teunis PFM, et al.** 2008. *Norwalk virus*: how infectious is it? J. Med. Virol. **80**:1468–1476.
34. **Thornley WR, Mumford DL.** 1979. Intracellular location of *Beet curly top virus* antigen as revealed by fluorescent antibody staining. Phytopathology **69**:738–740.
35. **van der Werf W, Hemerik L, Vlak JM, Zwart MP.** 2011. Heterogeneous host susceptibility enhances prevalence of mixed-genotype micro-parasite infections. PLoS Comput. Biol. **7**:e1002097. doi:10.1371/journal.pcbi.1002097.
36. **Zwart MP, Daros JA, Elena SF.** 2011. One is enough: in vivo effective population size is dose-dependent for a plant RNA virus. PLoS Pathog. **7**:e1002122. doi:10.1371/journal.ppat.1002122.
37. **Zwart MP, Daròs JA, Elena SF.** 2012. Effects of potyvirus effective population size in inoculated leaves on viral accumulation and the onset of symptoms. J. Virol. **86**:9737–9747.
38. **Zwart MP, et al.** 2009. An experimental test of the independent action hypothesis in virus-insect pathosystems. Proc. R. Soc. Lond. B Biol. Sci. **276**:2233–2242.